17th Brazilian Congress of Thermal Sciences and Engineering
November 25th-28th, 2018, Águas de Lindóia, SP, Brazil

ENCIT-2018-0030
ENERGY EFFICIENCY OF A SOLAR HEAT PUMP OPERATING IN NULL SOLAR RADIATION CONDITION

Hélio Augusto Goulart Diniz
Neylor Makalister Ribeiro Vieira
Stella Marys Silva Pinheiro
Universidade Federal de Minas Gerais, Mechanical Engineering Department, 31270091, Belo Horizonte, MG, Brazil
helioufmg@gmail.com; neylormakalister@yahoo.com.br; stella_marys_@hotmail.com

Matheus Henrique Gonzaga Niterói
University of Itaúna, School of Mechanical Engineering, Rodovia MG 431, Trevo Itaúna/Pará de Minas, 35680-142, Itaúna, MG, Brazil
matheushgn@gmail.com

Sabrina Nogueira Rabelo
Federal University of Minas Gerais, Graduate Program in Mechanical Engineering, Av. Antônio Carlos 6627, 31270-901 BeloHorizonte, MG, Brazil
University of Itaúna, School of Mechanical Engineering, Rodovia MG 431, Trevo Itaúna/Pará de Minas, 35680-142, Itaúna, MG, Brazil
sasanogueirarab@hotmail.com

Abstract. *The aim of this work is to carry out an analysis of the energy efficiency of an air-to-water heat pump with R134a refrigerant using experimental tests where the system operates with an immersion condenser and a solar evaporator without exposure to solar radiation. The heat rates exchanged with the solar evaporator and its efficiency were analyzed, as well as the coefficient of performance (COP) of the system. The heat pump COP was 2.29, considering the average of the five experiments conducted. The heating time of 200 liters of water from the average temperature of 32.0 ° C to 45.3 ° C was 4.3 hours. In addition, the evaporator showed to be well sized for the system, with an efficiency of 86%. This work made it possible to analyze the thermal behavior of a heat pump operating in a situation of low thermal energy availability.*

Keywords: Heat pump, water heating, solar evaporator, immersion condenser, heating pump.

1. INTRODUCTION

According to the study of energy efficiency and distributed generation for the years 2014 to 2024, 16.1% of the electric energy consumption of residences in Brazil in 2014 was generated for the use of electric showers. In 2015, this percentage was slightly reduced to 16.0%. The downward trend is expected in the coming years and the percentage could reach 14.5% in 2019 and 12.2% in 2024 (EPE, 2016a). There is an evolution perspective in the percentage of homes with solar water heating until 2024, showing the evolution of this type of energy in Brazilian homes. Given the increasing cost of energy production and the increasing consumption due to population growth, it is important to improve the energy efficiency and develop alternatives for production and improve equipment efficiency (EPE, 2016b).

A restriction on the use of the isolated solar collector system for water heating is the deficit of solar energy on some days of the year (rainy or cloudy weather), making the process of water heating unviable. Due to this aspect, it is necessary to share the solar collector with an auxiliary system for days of low solar incidence. Recent research has shown a good advantage in associating a heat pump with a solar collector system when environmental conditions are not favorable (Rodríguez et al., 2015).

One of the most promising technologies for replacing the electric showerhead in residential water heating is the use of the heat pump. A heat pump can work alone, providing savings in electricity consumption in relation to the shower, or it can function as auxiliary equipment in a solar collector system (Rodríguez et al., 2015; Silva et al., 2007). Rodríguez et al (2015) obtained an average annual performance coefficient (COP) of 1.88. Silva et al (2007) obtained an average COP of 2.01.

The trend we see in the literature is the use of the solar-type evaporator in heat pumps for water heating. This evaporator is exposed to solar radiation and therefore has a higher thermal power available compared to a closed

environment. Therefore, the COP of this type of heat pump is higher relative to the heat pumps that use other types of evaporators (Buker and Riffat, 2016; Omojaro and Breitkopf, 2013). However, situations in where the heat pump operates without sun exposure should be explored, as rainy or cloudy days that occur often in several regions.

A heat pump with solar evaporator can function as a solar collector regardless of the weather conditions of the day, as it still has good efficiency if it has not been exposed to solar radiation (Li et al., 2007; Li et al., 2007a; Li et al., 2007b). Willem et al (2017) obtained COPs of 4 to 4.9 in winter and 7 to 9 in summer for a CO2-fuelled water heating pump. Li et al (2007a) and Li et al (2007b) obtained a seasonal average COP of 5.25. Regarding the efficiency of the solar evaporator used in this type of system, Kong et al. (2011) obtained values ranging from 0.88 to 0.91.

The aim of this work is to carry out an analysis of the energy efficiency of the system based on experimental tests on an air-to-water heat pump with a solar evaporator operating without solar radiation. The heat pump works with the refrigerant fluid R134a as the primary fluid, with air as the secondary fluid in the evaporator and with water as the secondary fluid in the immersion condenser (coil tube immersed in a tank of water to be heated).

2. METHODOLOGY

The system components of the heat pump are detailed below, including the instrumentation used in the experimental evaluations, and the equations used to determine various parameters for analyzing the thermal behavior of the system.

2.1 Procedimentos experimentais

The heat pump operates according to the vapor compression cycle. In this system, the fluid working as hot source is the water stored in the tank and the cold source is the ambient air of a laboratory outside the influence of solar radiation. The cycle begins when ambient air powers the solar evaporator, transferring heat to the refrigerant fluid passing through this component. This fluid goes to the compressor, receiving the compression work in the form of heat, in addition to increasing the pressure, and then goes to the condenser. In this component, the cooling fluid, which transports the heat absorbed from the environment and the compressor, gives energy to the water. The water heats up and the refrigerator cools down. After this the refrigerant goes to the expansion valve, on where its pressure drops. It then returns to the same state in which it entered the evaporator, restarting the cycle.

The heat pump analyzed has two types of evaporators, a solar evaporator and a finned tube evaporator with forced ventilation. There are also two types of condensers available, one coaxial countercurrent and one immersion capacitor. The system operates with a hermetically sealed reciprocating compressor (1/3 HP rated power), a thermostatic expansion valve type expansion device and a coolant reservoir bottle. The heat pump circuit has a number of valves that control the flow of refrigerant fluid through the heat exchangers in such a way that it allows the operator to select only one evaporator and one condenser to operate. Finally, the heat pump has a thermal tank (tank) with a storage capacity of 200 liters of water. The tank is full and the immersion condenser heats the water from a temperature of about 32°C to about 45°C. Figure 1 shows the view of the cooling cycle system, instrumented with Bourdon manometers and thermocouples K, with the main components except the thermal tank.

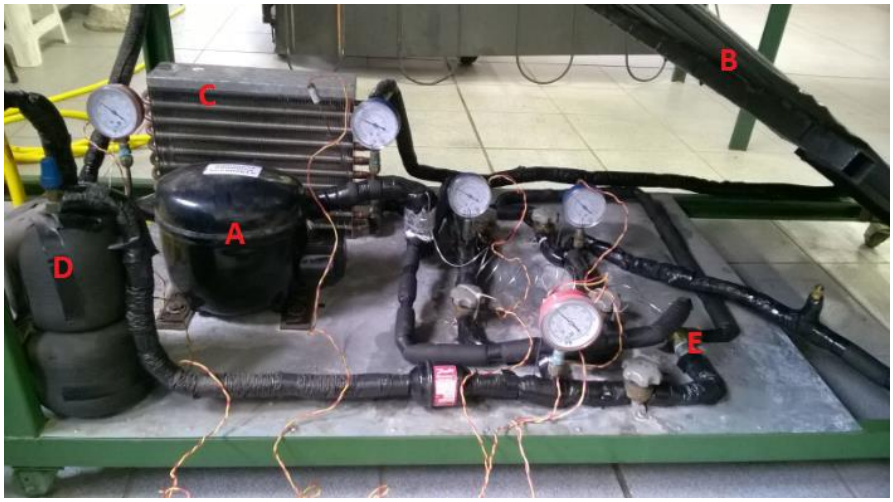

Figure 1. Refrigeration cycle system view. (A) Compressor, (B) Solar evaporator, (C) Finned tube evaporator, (D) Thermal back up bottle and (E) Thermostatic valve.

Figure 2 shows the macro view of the heat pump in addition to the construction data of the solar evaporator. The thermal water tank and the solar evaporator (103x160 mm) are also shown.

Tube material	Copper
Plate material	Aluminum
Inner tube diameter	8.73 mm
Outer tube diameter	9.53 mm
Plate thickness	1 mm
Length of the tube (without curves)	16.0 m
Extended length of curves	1.28 m
Plate width	1.03 m
Plate length	L_{pl} = 1.60 m
Plate area	A_{pl} = 1.65 m²
Plate Emissivity	ε = 0.95

Figure 2. Heat pump macro view and solar evaporator constructive data.
(A) Solar evaporator and (B) Water reservoir.

The solar evaporator was installed at a fixed angle of 30º to perform the tests and below it was installed with a condensed water collection system that runs and accumulate in a water gutter in the lower portion, as shown in Fig. 3. A graduated cylinder measured the volume of the condensed water generated.

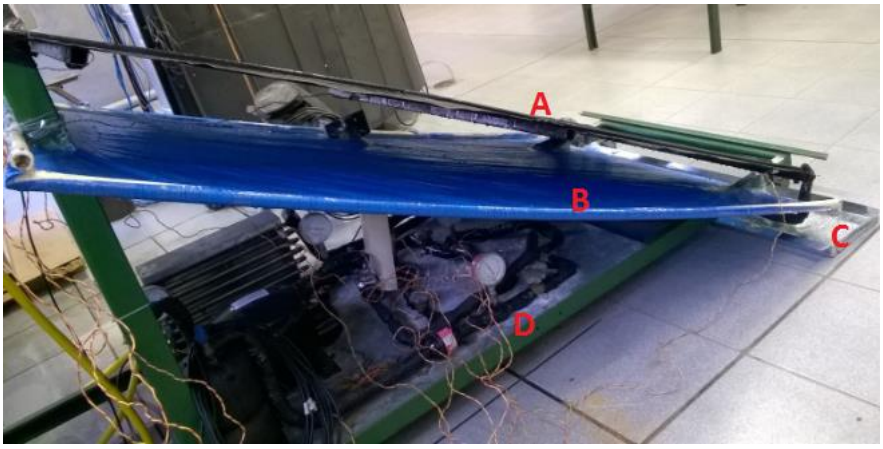

Figure 3. Side view of the heat pump. (A) Solar evaporator, (B) Condensed collector system, (C) Condensed accumulator and (D) Refrigeration cycle system.

A device was designed and installed to collect condensed water vapor on the plate. The condensate was being formed on both sides of the plate. On the anterior face, the condensate would drip and fall on the lower portion of the plate. However, in the plate posterior face there was a constant dripping throughout its extension (due to the inclination), requiring the implantation of a collection device, a kind of waxed canvas positioned below the plate (far enough away from it not to interfere with the heat exchange) so that the condensate could fall on it and be drained into the lower area of the plate. In the lower portion of this was placed a condensate storage gutter, which covered the entire width of the plate, ensuring that all condensate formed was collected.

The solar evaporator is a serpentine-fin assembly (tubular plate) built for the use of natural convection imposed by ambient air, solar radiation and the environment and also the latent heat of condensation of water vapor present in the air. The plate temperature was recorded by three K-type thermocouples, two of which were positioned in the regions near the extremities and the other in the central region.

Figure 4 shows the detail of the tank bottom with the internal view (where it is possible to see the immersion condenser). The construction data of the component is also shown. A psychrometer was used to collect ambient temperature and dew point temperature data on water vapor in the air. A power meter was used to monitor the real energy consumption of the compressor.

Tube material	Copper
Inner tube diameter	8.73 mm
Outer tube diameter	9.53 mm
Tube length	4.5 m

Figure 4. Internal view of the tank where the condenser is immersed. Condenser in serpentine shape and constructive data of the component.

The water temperature in the reservoir was determined by the average of three different measurements done in three different locations, in the lower, middle and upper region of the tank. It used K thermocouples to do the measurements. The interval between measurements of the quantities involved in the operation of the system was 15 minutes. The measured values were: temperatures and pressures of the thermodynamic vapor compression cycle, water temperature, ambient temperature, plate and dew point, the electrical energy consumed by the compressor and the volume of water vapor condensate generated.

The measurement uncertainties are organized in Tab. 1 according to the instruments manuals.

Table 1. Instruments measurement uncertainty.

Measuring instrument	Uncertainty
K Thermocouple	$\pm$ 1 ºC
Bourdon gauge (low pressure)	$\pm$ 0.1 bar (1% full scale)
Bourdon pressure gauge (high pressure)	$\pm$ 0.35 kgf/cm² (1% full scale)
Digital psychrometer	$\pm$ 1 °C (ambient temperature)
	$\pm$ 2 °C (dew point temperature)
Power Meter	$\pm$ 1%
Tester	$\pm$ 2 ml
Tank	$\pm$ 5%

2.2 Modeling procedures

The thermal performance, $\mathrm{COP}_{\mathrm{global}}$, of the heat pump was determined by Eq. 1, where m_a is the mass of water, ΔT_a is the temperature variation of the water (final and initial state), c_{p_a} is the specific heat of water at constant pressure, $\dot{W}_{comp_{real}}$ is the real compressor work and t is the measurement time (15 minutes).

$$\mathrm{COP}_{\mathrm{global}} = \frac{m_a c_{p_a} \Delta T_a}{\dot{W}_{comp_{real}} t} \tag{1}$$

It was considered that all the heat supplied by the condenser $\dot{Q}_{cond}$ as it passes through the condenser is fully absorbed by the water in the tank. Thus, all the heat losses occurred by the tank were neglected. The heat rate $\dot{Q}_{cond}$ is given by Eq. 2, where $h_{f_{cond_{\mathrm{out}}}}$ and $h_{f_{cond_{ent}}}$ are, respectively, enthalpies of the refrigerant fluid at the outlet and inlet of the condenser. In addition, $\dot{Q}_{cond}$ can be evaluated as the heating capacity of the system. Finally, $\dot{m}_f$ is the mass flow rate of refrigerant through the system.

$$\dot{Q}_{cond} = \dot{m}_f (h_{f_{cond_{ent}}} - h_{f_{cond_{\mathrm{out}}}}) \tag{2}$$

The thermal cycle performance of the heat pump COP_{cycle} is given by Eq. 3, where $\dot{W}_{comp_{ideal}}$ is the ideal work of the compressor given by Eq. 4 and $h_{f_{evap_{\mathrm{out}}}}$ is the enthalpy of the refrigerant fluid at the evaporator outlet.

$$\mathrm{COP}_{cycle} = \frac{\dot{Q}_{cond}}{\dot{W}_{comp_{ideal}}} \tag{3}$$

$$\dot{W}_{comp_{ideal}} = \dot{m}_f (h_{f_{cond_{ent}}} - h_{f_{evap_{\mathrm{out}}}}) \tag{4}$$

The ideal work of the compressor considers only the thermodynamic cycle carried by the refrigerator. It does not take into account the losses inside the compressor, such as heat losses to the external environment and losses due to irreversibilities. Thus, $\dot{W}_{comp_{ideal}}$ is smaller than $\dot{W}_{comp_{real}}$, this culminates that the COP_{cycle} is larger than the overall thermal performance $\mathrm{COP}_{\mathrm{global}}$ of the heat pump. The thermal performance of the heat pump that really matters is provided by $\mathrm{COP}_{\mathrm{global}}$, as considered in all the works present in the literature. Considering this, it is possible to evaluate how efficient the system is used. In addition, the overall efficiency of the compressor η_{comp} can be given by Eq. 5.

$$\eta_{comp} = \frac{\dot{W}_{comp_{ideal}}}{\dot{W}_{comp_{real}}} = \frac{\mathrm{COP}_{global}}{\mathrm{COP}_{cycle}} \tag{5}$$

Tests performed with the heat pump operating without solar radiation (in the laboratory), simulating rainy or cloudy days, resulted in the formation of condensate of water vapor in the collector (solar evaporator). Thus, the rate of latent heat of air, $q_{cond_{steam}}$, was considered. The contribution by the sensible heat of the air q_{conv}, due to the natural convection of the air around the collector, and the radiation of the environment q_{rad}, were also considered. These three portions of heat exchanges were responsible for the thermal input of the available environment for the collector when it is operated indoors (laboratory). It should be noted that the heat rate due to solar radiation was considered non-existent for this operating situation. The mathematical modeling of the three heat rates responsible for heat transfer with the collector will be performed according to references in the specialized literature.

The efficiency of the collector η_{col}, given by Eq. 6, is evaluated by the relation between the heat rate absorbed by the refrigerant fluid when passing through the evaporator $\dot{Q}_{evap_{real}}$, given by Eq. 7, and the environment available heat rate which could theoretically be absorbed by the collector $\dot{Q}_{evap_{ideal}}$, given by Eq. 8. Where $h_{f_{evap_{ent}}}$ is the enthalpy of the refrigerant fluid at the evaporator inlet. $\dot{Q}_{evap_{real}}$ can be assumed as capacity of the refrigerant fluid to absorve energy from the environment as it passes through the evaporator.

$$\eta_{\mathrm{col}} = \frac{\dot{Q}_{\mathrm{evap_{real}}}}{\dot{Q}_{\mathrm{evap_{ideal}}}} \tag{6}$$

$$\dot{Q}_{evap_{real}} = \dot{m}_f (h_{f_{evap_{\mathrm{out}}}} - h_{f_{evap_{ent}}}) \tag{7}$$

$$\dot{Q}_{evap_{ideal}} = q_{cond_{steam}} + q_{rad} + q_{conv} \tag{8}$$

The η_{col} provides an important parameter to evaluate the energy efficiency of the collector, representing the percentage heat coming from the environment that is received by the collector and used by the refrigerator in its expansion when passing through the evaporator. It also indicates how well the collector is sized for the operating system under certain conditions.

2.2.1 Solar evaporator heat exchange modelling

The natural convective coefficient $H_{conv_{nat}}$ is given by Eq. 9.

$$H_{conv_{nat}} = \frac{Nu_{conv_{nat}} k_{air}}{L_{pl}} \tag{9}$$

Where k_{air} is the air thermal conductivity coefficient at the mean temperature between the plate and air (film temperature), L_{pl} is the plate length and $Nu_{conv_{nat}}$ is the Nusselt number for the natural convection. The latter is given by Eq. 10.

$$Nu_{conv_{nat}} = \left\{ 0{,}825 + \frac{0{,}387 Ra^{1/6}}{\left[1+(0{,}492/Pr_{air})^{9/16}\right]^{8/27}} \right\}^2 \tag{10}$$

Where Pr_{air} is the air Prandtl number at the film temperature and Ra is the Rayleigh number given by Eq. 11.

$$Ra = \frac{g cos\theta \beta (T_{air} - T_{pl}) L_{pl}^3}{\alpha_{air} \upsilon_{air}} \quad (11)$$

Where g is the gravity acceleration (9.81 m / s²), θ is the plate inclination angle with the vertical (60 °), β is the thermal volumetric expansion coefficient (calculated by the film absolute temperature inverse (Kelvin)), T_{air} is the air temperature, T_{pl} is the average plate temperature, α_{air} is the air thermal diffusivity and υ_{air} is the air kinematic viscosity, both at the film temperature.

The ambient radiation coefficient H_{rad} is given by Eq. 12.

$$H_{rad} = \varepsilon \sigma (T_{viz} + T_{pl})(T_{viz}^2 + T_{pl}^2) \quad (12)$$

Where σ is the Stefan-Boltzmann constant (5.67 x 10-8 W / m².k4) and T_{viz} is the surrounding temperature, considered equal to the air temperature.

The ambient radiation heat rate q_{rad} exchanged by the evaporator and the surrounding is given by Eq. 13.

$$q_{rad} = H_{rad}(2A_{pl})(T_{viz} - T_{pl}) \quad (13)$$

Where A_{pl} is the board one-sided area. The two faces of the plate were considered to exchange heat by ambient radiation, natural convection and by condensation.

The natural convection heat rate q_{conv} is given by Eq. 14.

$$q_{conv} = H_{conv_{nat}}(2A_{pl})(T_{air} - T_{pl}) \quad (14)$$

The theoretical condensation heat rate $q_{cond_{vapor_{\text{theoretical}}}}$ of the water vapor present in the air upon condensation on the evaporator surface is given by Eq. 15 to Eq. 17.

$$q_{cond_{vapor_{\text{theoretical}}}} = H_m(2A_{pl})(P_v - P_{sat})h_{lv_a} \quad (15)$$

$$H_m = \frac{H conv_{nat}}{c_{p_{air}} \rho_{air} R_{a_v} T_{air}} \left(\frac{P_{air}}{P_v - P_{sat}}\right) In \left[\frac{P_{air} - P_{sat}}{P_{air} - P_v}\right] \quad (16)$$

$$P_v = \phi P_{sat} \quad (17)$$

Where $c_{p_{air}}$ is the air specific heat at constant pressure and ρ_{air} the air specific mass, both measured at room temperature. In addition, P_{air} is the atmospheric pressure, P_v is the partial vapor pressure in the air measured at the air temperature, and P_{sat} is the vapor saturation pressure measured at the plate temperature. Finally, $R_{a_v} = 461{,}5\, J/kg.K$ is the gas constant of the water vapor. However, in Eq. 17, P_{sat} is evaluated at room temperature. Furthermore, ϕ is the relative humidity of the air. The dew point temperature T_o is provided by the psychrometer and is related to the local atmospheric pressure, air relative humidity and ambient temperature. These parameters are fundamental for the determination of P_v and P_{sat} through the EES.

Scarpa and Tagliafico (2016) used Eq. 15 to 17 in their research. These equations take into account the dilution of water vapor in air in the atmosphere. This approach consisted in calculating the mass transfer coefficient H_m for the condensation of a very dilute system on a cold surface, based on the analogy of heat transfer and mass, from the knowledge of the convective heat transfer coefficient $H_{conv_{nat}}$ at the air and board interface.

The condensate was collected at each interval of 1 hour and its volume measured by a beaker. The temperature of this water was already close to the ambient temperature, because the time that it takes to be stored in the gutter is sufficient for stablishing the thermal equilibrium with the environment. Thus, it was possible to perform the experimental measurement of the condensate, performing a similar work to that of Scarpa and Tagliafico (2016), in which it served as a basis for comparison of the results.

Thus, the mass flow of the experimental condensate $\dot{m}_{cond_{exp}}$ is given by Eq. 18.

$$\dot{m}_{cond_{exp}} = \frac{\rho_{cond} Vol_{cond}}{t} \quad (18)$$

Where ρ_{cond} is the liquid water specific mass at room temperature and Vol_{cond} is the volume of water collected during time period t.

The condensate mass flow rate can also be calculated, thus being called the theoretical value $\dot{m}_{cond_{\text{theoretical}}}$ and given by Eq. 19.

$$\dot{m}_{cond_{\text{theoretical}}} = \frac{q_{cond_{steam_{\text{theoretical}}}}}{h'_{lv_a}} \quad (19)$$

Where the water modified liquid vapor enthalpy h'_{lv_a} is given by Eq. 20.

$$h'_{lv_a} = h_{lv_a} + 0{,}68 c_{p_{l_a}}(T_o - T_{pl}) \quad (20)$$

Where h_{lv_a} is the liquid water vapor enthalpy measured at the dew point temperature and $c_{p_{l_a}}$ is the saturated liquid water specific heat at constant pressure and at the film temperature.

Likewise, the experimental or real water vapor condensation rate $q_{cond_{steam}}$ can be determined by Eq. 21.

$$q_{cond_{steam}} = \dot{m}_{cond_{exp}} . h'_{lv_a} \quad (21)$$

The theoretical and experimental values were compared, analyzing the difference of values between them and how well the literature modeling describes the real situation.

Finally, the EES (Engineering Equation Solver) software was used for the acquisition of all the properties of the fluids and solids described throughout the work.

3. RESULTS AND DISCUSSION

Five water tank heating tests were performed. The values of the quantities given below refer to the average of the values obtained in these tests. In addition, we performed the uncertainty propagation analysis for the COP_{real}, the most important magnitude of the system.

The water was heated from the average temperature of 32.0 °C to the average temperature of 45.3 °C, the average ambient temperature was 26.8 °C. The average plate temperature was 9.2 °C. In addition, the average test time was 4h18min and it was performed an average of 18 measurements of the variables per test. The water heating curve during the test time will be plotted to identify the trend of the system over time.

The water heating curve over the test time is shown in Fig. 5 to identify the trend of the system over time.

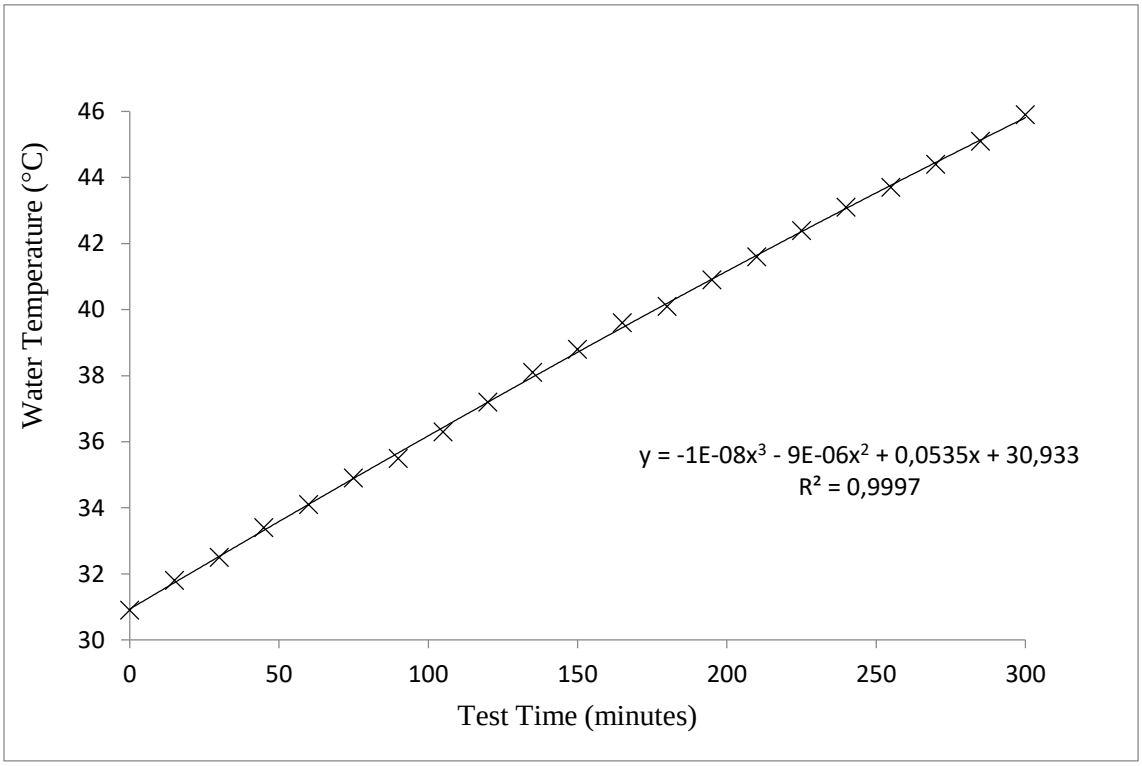

Figure 5. Water heating (4th test).

The cycle performance coefficient, on average, was 4.26 and the global, on average, was 2.29 ± 0.05 and its uncertainty propagation was determined. Figure 6 shows the COP curves as a function of water heating. The system

thermal performance, for both the cycle and the global, suffered a degradation with water heating, ranging from 4.74 to 3.86, on cycle COP average, and varying from 2.52 to 1, 95, on global COP average.

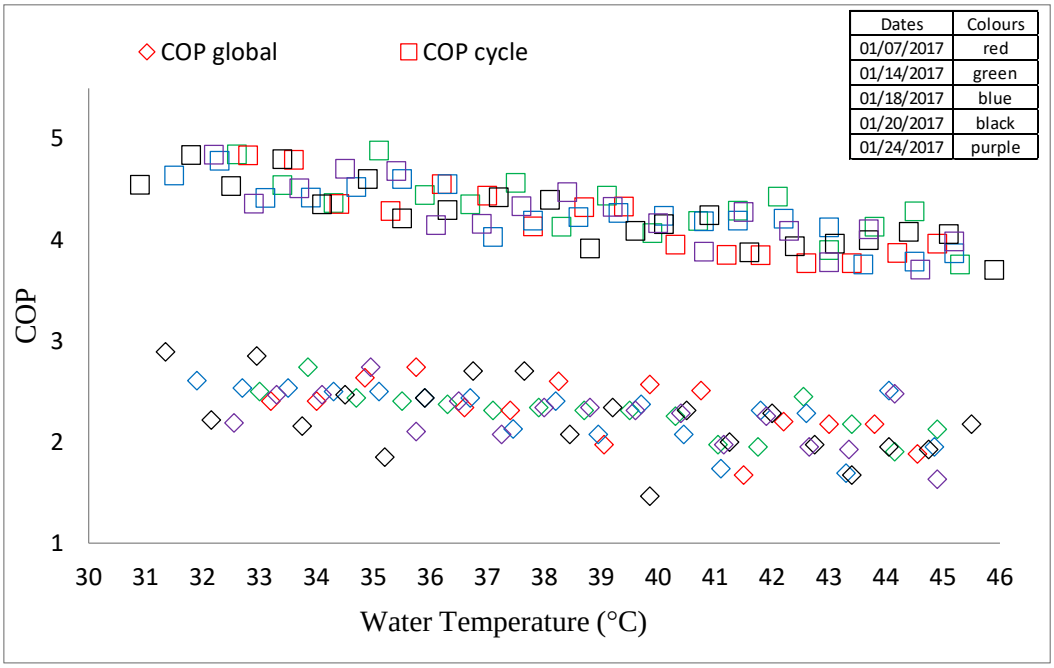

Figure 6. System thermal performance.

The average collector efficiency was 0.86 and the contribution of the average heat rate provided by the water vapor condensation (experimental) present in the air to the collector was 26% of the total (the remainder is due to ambient radiation and convection). Figure 7 presents the results of these parameters.

The efficiency of the collector was, on average, 86%, a value that agree with the specialized literature. A value that means the good collector design for the system when it operates in a situation of zero solar radiation.

The global thermal performance was 0.53, with the general tendency to remain constant. The average ideal work of the compressor was 168 W, varying on average from 156 W to 169 W. The average real work of the compressor was 316 W, varying on average from 294 W to 341 W, according to Figure 8. The compressor ideal work (power) had a slight growth tendency; however, there was a continuous and significant increase in the real power of the compressor with the water heating, which caused the system thermal performance degradation.

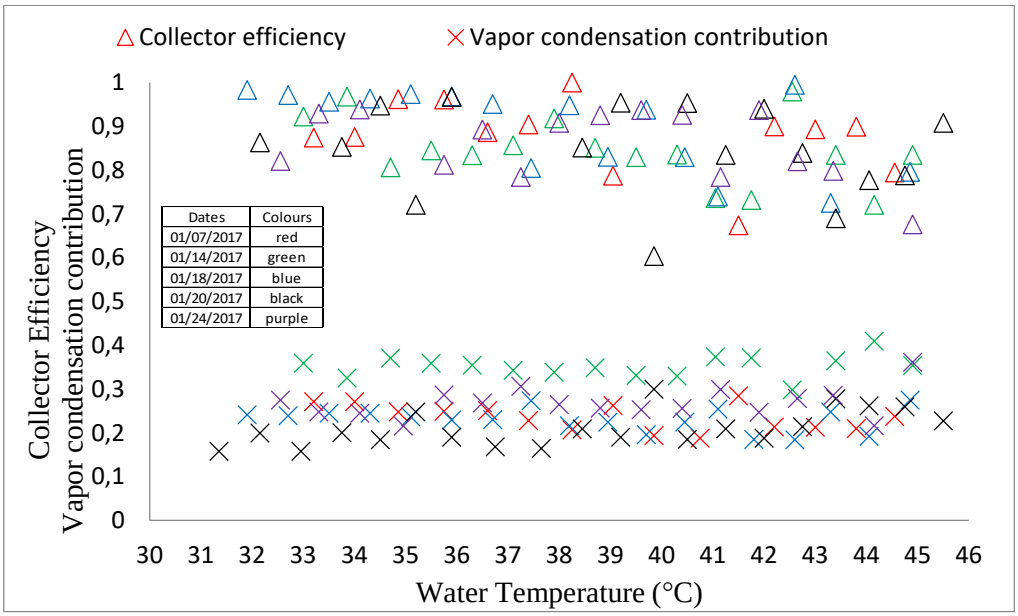

Figure 7. Collector thermal efficiency and vapor condensation contribution.

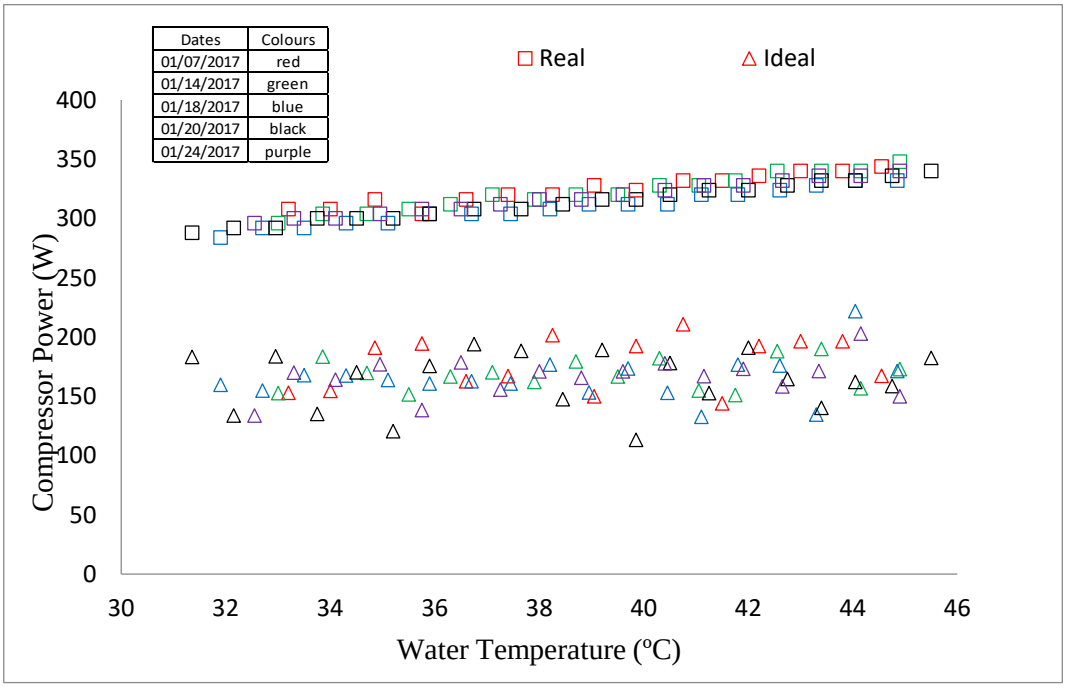

Figure 8. Compressor work.

The average heat rate harnessed from the environment $\dot{Q}_{evap_{real}}$ was 549 W and the average system heating capacity $\dot{Q}_{cond}$ was 718 W. The heat rate due to ambient radiation and the air sensible heat rate are presented in Fig. 9. The theoretical heat rate by radiation was predominant in relation to the others and had an average contribution of 50% of the collector available total. The latent heat theoretical rates (average of 23%) and sensible heat (average of 27%) complemented the rest of the participation.

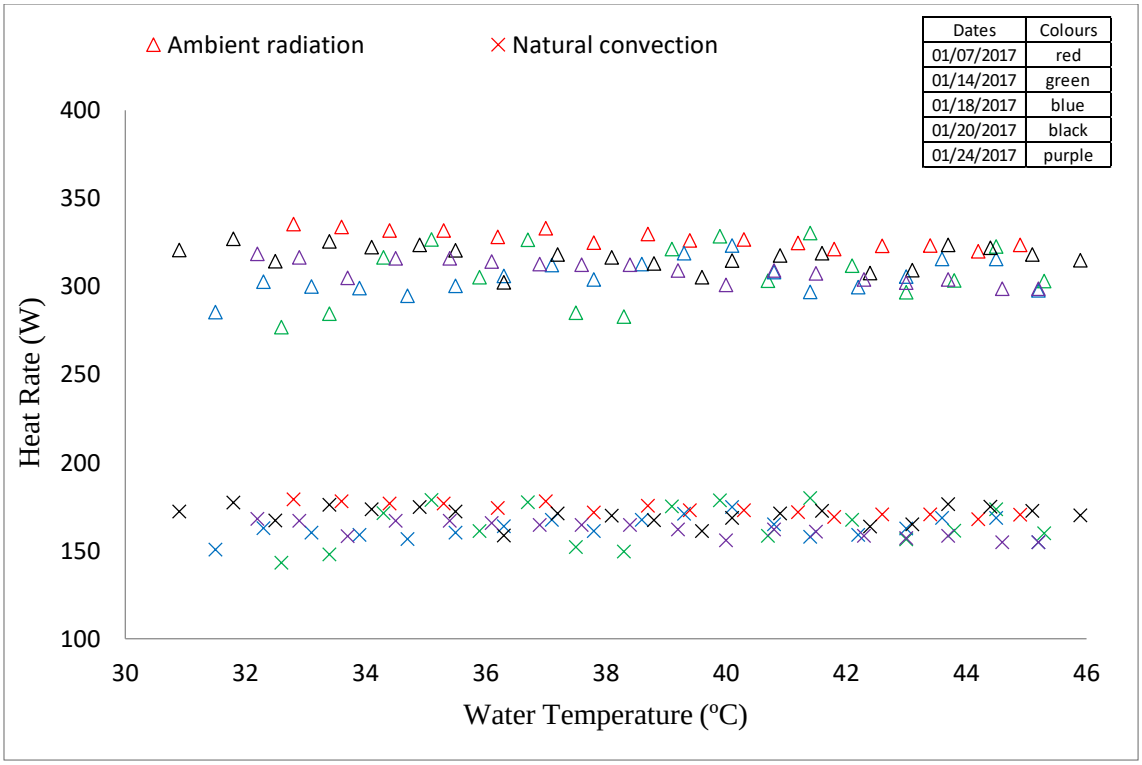

Figure 9. Heat rates by natural convection and by ambient radiation.

The theoretical and real latent heat rates presented variable profiles and depended on relative humidity. However, the mean difference between these rates was 5.7%, that is, by using the literature equations, a mean value was obtained that was slightly lower than the real one. Concerning condensate rate formed, the estimated value using the presented literature equations resulted in an average difference of 9.5%. These percent results represent low average errors.

4. CONCLUSIONS

This work allowed analyzing the energy efficiency of a solar heat pump operating in a situation of non-existence of solar radiation from the sun. It reflects cloudy or rainy weather conditions, in which the solar thermal contribution is negligible and the solar evaporator only has the energy present in the environment.

The five tests carried out and analyzed identified a satisfactory functioning of the heat pump, carrying out the heating of 200 liters of water in the average temperature range of 32.0 °C to 45.3 °C in an average time of 4.3 hours. It has an average heating capacity of 718 W and a thermal performance of 2.29±0.05. The collector was well sized for the environmental conditions of the tests, presenting an efficiency of 86%.

The results of this research reinforce the advantages of using a water heating system with a heat pump, even when operating with a solar evaporator not exposed to solar radiation. The system was shown to be advantageous in relation to the traditional residential water heating equipment in Brazil (electric water heater) that has a maximum COP equal to 1.

5. REFERENCES

Buker, M.S. and Riffat, S.B., 2016. “Solar assisted heat pump systems for low temperature water heating applications: A systematic review”. *Renewable and Sustainable Energy Reviews*, Vol. 55, p. 399-413.

EPE - Empresa de Pesquisa Energética, 2016a. “Eficiência Energética e Geração Distribuída para os próximos 10 anos (2015-2024)”, Rio de Janeiro, Brazil.

EPE - Empresa de Pesquisa Energética, 2016b. “BEM: Balanço Energético Nacional de 2016”, Rio de Janeiro, Brazil.

Incropera, F.P., Dewitt, D.P., Bergman, T.L. and Lavine, A.S., 2007. *Fundamentals of Heat and Mass Transfer*. John Wiley and Sons, Hoboken, 6th edition.

Kong, X. Q., Zhang, D., Li, Y. and Yang, Q. M., 2011. “Thermal performance analysis of a direct-expansion solar-assisted heat pump water heater”. *Energy*, Vol. 36, p. 6830-6838.

Li, Y.W., Wang, R.Z., Wu, J.Y. and Xu, Y.X., 2007a. “Experimental performance analysis on a direct-expansion solar-assisted heat pump water heater” *Applied Thermal Engineering*, Vol. 27, p. 2858-2868.

Li, Y.W., Wang, R.Z., Wu, J.Y. and Xu, Y.X., 2007b. “Experimental performance analysis and optimization of a direct expansion solar-assisted heat pump water heater”. *Energy*, Vol. 32, p. 1361-1374.

Omojaro, P. and Breitkopf, C., 2013. “Direct expansion solar assisted heat pumps: A review of applications and recent research”. *Renewable and Sustainable Energy Reviews*, Vol. 22, p. 33-45.

Rodríguez, O.R.S., Koury, R.N.N. and Maia, A.A.T., 2015. “Socio-economic performance of a solar flat plate collector based in a heat pump water heating system in the brazilian southeast region”. *International Congress of Mechanical Engineering – COBEM*. Rio de Janeiro, Brazil.

Silva, I.C., Oliveira, R.N., Koury, R.N.N. and Machado, L., 2007. “Análise da viabilidade econômica e estudo do desempenho de uma bomba de calor ar-água como apoio ao sistema de coletor solar.” *Congresso Iberoamericano de Engenharia Mecânica*. Cusco, Peru.

Willem, H., Lin, Y. and Lekov, A., 2017. “Review of energy efficiency and system performance of residential heat pump water heaters” *Energy and Buildings*, Vol. 143, p. 191-201.

6. RESPONSIBILITY NOTICE

The authors are the only responsible for the printed material included in this paper.